Rev. Roum. Sci. Techn.– Électrotechn. et Énerg.
Vol. **62**, *4*, pp. 352–357, Bucarest, 2017

HEAT TRANSFER ANALYSIS OF AN AXIAL FLUX SYNCHRONOUS WIND GENERATOR USING 3D FINITE ELEMENT MODELS

OVIDIU CRAIU, TIBERIU TUDORACHE

Key words: Heat transfer, Finite element method, Synchronous generator, Permanent magnets.

This paper presents some practical aspects regarding heat transfer analysis inside a permanent magnet synchronous machine used in wind conversion systems. Two steady state models were developed using COMSOL Multiphysics software package and compared. The influence of the heat conductivities of component materials and conduction coefficients upon the final results was analyzed. A transient 3D model was developed to study special cases when the generator operates at high intermittent currents (*e.g.* during harsh winds) and how that influences the heat transfer and temperature distribution inside machine.

1. INTRODUCTION

The avail of wind power for generating electricity has gradually increased during last decades. This growing trend has been strongly encouraged by targeted policies in favor of renewable and clean energies, adopted by different countries and international institutions. As a result, at the end of 2016, about 10.4 % of the electricity consumption in EU was from wind generation [1].

The wind power is transformed into electricity by wind energy conversion systems (WECS) built in a wide range of powers and constructive solutions. The main element of WECS, the electric generator, is typically a synchronous or asynchronous machine with radial magnetic flux, or, sometimes, with axial flux [2–5]. The interest in the latter has grown especially during the last decade [6, 7], these machines being less analyzed than those with radial flux.

The axial flux permanent magnet (AFPM) machines have several advantages: high torque density, reduced amount of active materials, high efficiency and modular construction [7]. They are preferred in domains like the automotive industry and WECS [8].

This paper presents a study of the heat transfer in a slot-less AFPM synchronous generator used in a small power direct drive wind turbine (*i.e.* without gearbox). The numerical investigation is based on the finite element method (FEM), and was carried out using the professional software package COMSOL Multiphysics ®.

2. SHORT DESCRIPTION OF STUDIED AFPM GENERATOR

The studied AFPM synchronous generator has a compact design, with rated power S_n = 1 kVA, rated current I_n = 4 A, $2p$ = 20 poles and operates at rated speed n_n = 300 rpm. It is energized by permanent magnets (PMs) mounted on two iron disks placed on the sides of a slot-less toroidal stator holding the windings (Fig. 1). The stator coils are wound around the iron core resulting in theoretically no cogging torque. The stator iron core is made of grain oriented electric steel laminations characterized by reduced iron losses, leading to a high efficiency.

Given the AFPM high power density and taking into account that iron and Joule losses are dissipated in the stator, which is sandwiched between the two rotors making the cooling more difficult, a thorough heat transfer analysis was necessary to verify the maximum temperatures.

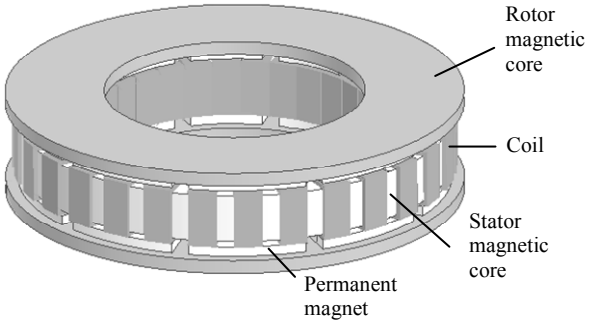

Fig. 1 – Example of AFPM generator with main active parts emphasized.

3. HEAT TRANSFER MODEL

The studied AFPM presented in Fig. 2 has 30 coils, each with 84 turns, while the two rotors are both equipped with 20 NdFeB PMs, with facing magnets of same polarity. The geometric data of the generator are provided in Table 1.

Table 1

Main geometrical data of the AFPM synchronous generator

Outer diameter of stator core [mm]	350
Inner diameter of stator core [mm]	230
Height of stator core [mm]	40
Outer diameter of rotor yoke [mm]	369.6
Height of rotor yoke [mm]	11
Chassis outer diameter [mm]	385.6
Chassis outer height [mm]	112

Due to its physical symmetries, the FEM heat transfer computation domain was reduced to 1/20th of the entire machine geometry. It consists of a 36° sector that corresponds to one pole pair, cut through the middle of the stator (Fig. 2).

Using the professional FEM based software COMSOL Multiphysics, the temperature T distribution was computed solving the heat transfer equation in solids [9]:

$$\gamma C_p \frac{\partial T}{\partial t} + \nabla \cdot \mathbf{q} = Q$$
$$\mathbf{q} = -k \nabla T, \tag{1}$$

where γ is the material density [kg/m^3], $\mathbf{q}$ – the thermal flux [W/m^2], C_p – the specific heat capacity [kJ/kg/ºC], Q – the heat source [W/m^3], k – the thermal conductivity [W/m/ºC].

"Politehnica" University, Electrical Engineering Faculty, Bucharest, E-mail: ovidiu.craiu@upb.ro; tiberiu.tudorache@upb.ro

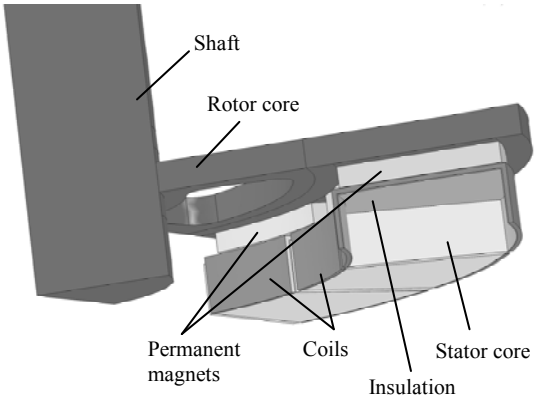

Fig. 2 – The computation domain and main regions of AFPM generator (air, chassis and partly the iron core regions were removed for better viewing).

The studied AFPM wind generator has a totally enclosed configuration, which provides a better weather protection, but a worse cooling compared to a through-flow ventilated rotor-stator system. As the outer surface of the generator chassis is in direct contact with the ambient air, this ensures a better external cooling compared to generators that have additional enclosures.

While modeling the heat transfer through conduction inside the solid parts of the generator is rather straightforward, the analysis of the heat transfer in the air regions is more challenging. Many models and empirical approximations have been made so far in order to better approximate the heat transfer through air, depending on the air cavity shape, the speed and air pressure etc. [11, 12]. In particular, for the current model, there were two types of air regions considered: a) the disk regions *i.e.* the region between the rotor and stator disks and the region between the rotor and the inside disk surface of the chassis, and b) the cylindrical regions (annuli) formed by the machine shaft and the inner side of the rotor, and between the rotor outer cylindrical surface and the inner chassis lateral cylinder.

Most of the known models do not particularly fit the current one, especially for the air "disk type" regions located between the generator shaft and the stator [12–14]. The revolving magnets act as a propeller moving the air inside the generator enclosure, adding to the model complexity. The rotor speed was assumed equal to the rated speed, although, in real life speed changes according to the wind velocity, which modifies both the heat transfer inside the generator, as well as the cooling conditions (*i.e.* the heat transfer coefficient) on the outer surface.

Two 3D FEM heat transfer models have been developed, approximating differently the heat transfer through the air. A discussion and comparison of the two models in regard to the selection of the thermal conductivity and convective heat transfer coefficients, are presented.

Variant A – Considers heat transfer in the inner air regions by both conduction and convection through an equivalent thermal conductivity. This is done in the model by multiplying the air thermal conductivity $k = 0.025$ W/m/ºC, with Nusselt number Nu:

$$\mathrm{Nu} = \frac{D_h h_c}{k}, \tag{2}$$

where h_c is the heat transfer coefficient by convection [W/m^2/ºC] and D_h is the equivalent hydraulic diameter [m] computed as:

$$D_h = 4A_c / p, \tag{3}$$

A_c is the effective flow area and p is the perimeter of the annulus rectangular cross section.

The type of air flow, either laminar or turbulent, depends on Reynolds number, as does Nusselt number, and both depend on the fluid (air) velocity. Reynolds number is computed as:

$$\mathrm{Re} = \frac{\Omega g R}{\nu}, \tag{4}$$

with Ω the angular velocity [rad/s] of the rotor, g is the gap between rotor and stator in [m], R the radius of the annuli, corresponding to the moving cylinder (*i.e.* the outer radius of the rotor for the annulus formed between the chassis and rotor cylinders, and the inner stator radius for the annuli formed between the stator and shaft cylinders) in [m] and ν is the kinematic viscosity of the fluid [m^2/s]. Given the reduced angular speed of the rotor (with rated value 31.4 rad/s, corresponding to a rotational speed of 300 rpm), and taking into account the geometrical dimensions of the model, the flow of the fluid results laminar [16].

The heat transfer in the air-gap region of disk type systems (*i.e.* axial machines) was studied by numerous researchers, based on a model consisting in a large diameter disk rotating freely in a fluid [15]. These disk systems were studied with or without superposed flow, for opened or enclosed systems [15–17] and allowed determination of Nusselt number for different airgap – radius ratios, at given rotational speed. Similarly, Nusselt numbers for the air "cylindrical type" regions were estimated based on Taylor-Couette correlations [16].

The Nusselt numbers used for the *Variant A* model are shown in Table 2.

Table 2

Nusselt numbers for all air-regions

Nu	Air region
6.7	Between rotor and chassis disks
7.5	Between rotor and stator disks (in areas with no magnets)
2.0	In the air-gap
2.7	Between rotor cylinder and chassis
3.5	Between inner surface of the stator and shaft

On the outer surfaces of the model the heat transfer was considered through a convective heat flux:

$$q_o = h_c(T_{ext} - T), \tag{5}$$

taking T_{ext} = 20°C, the exterior air temperature. Due to the unpredictable wind speed and direction, the cooling of the generator chassis was modeled using an average, constant value of h_c = 10 W/m^2/°C.

Variant B – Air regions inside generator are considered isothermal, with no convection and radiation taken into account on the contact with solid surfaces. As the movement of the rotor equipped with protruding magnets acts like a fan inside the machine, that engages the air a rotational move, which homogenizes its temperature. For this reason, in *Variant B* model the air-regions are considered isothermal. Thus, the heat is transferred only through forced convection, which depends on temperature difference between air and solid walls in contact with. The air temperature is determined iteratively from a heat flux balance equation:

$$\int_S \mathbf{q}\cdot\mathbf{n}\mathrm{d}S = \int_{vol} Q\mathrm{d}v. \quad (6)$$

As there is no heat source in the air, the right term in eq. (6) vanishes and the total heat flux is zero – i.e. the heat transferred by convection to the air from the warmer walls equals the heat transferred further from the air to the cooler walls. From a numeric point of view, in this formulation, the air regions are practically "extracted" from the computation domain and replaced with convective fluxes on the contact surfaces with the solid walls.

Due to its small size, and given the fact the heat transfer is mostly due to conduction, the air-gap was modeled the same way as in Variant A model, using an equivalent conduction coefficient multiplied by Nusselt number Nu = 2.02.

In order to maintain consistency between the two models, the convective coefficients on the air-solid contact surfaces used in Variant B model were determined from eq. (2), based on the Nusselt numbers used in Variant A model. The coefficient values are shown in Table 3.

Table 3

Convective coefficients on the solid walls

Convection coefficient [W/m^2/°C]	Surface
$h_{cS1} = 3$	Shaft surface
$h_{cS2} = 3$	Inner stator surface
$h_{cS3} = 15$	Rotor disk lower surface
$h_{cS4} = 17$	Chassis disk inner surface
$h_{cS5} = 17$	Rotor disk upper surface
$h_{cS6} = 18$	Rotor disk external cylinder side
$h_{cS7} = 18$	Inner chassis cylinder

4. NUMERICAL RESULTS

Taking into account the physical symmetries, the computation domain was reduced to 1/20th of the generator (Fig. 3). The FE computation domain was divided into 1, 125, 114 quadratic tetrahedrons to ensure sufficient elements in the areas of high temperature gradient. Particularly, a fine mesh discretization was used to model the insulation placed between the stator coils and the iron core and also for the air-gap region (Fig. 3).

Joule losses. The heat source was computed from the electromagnetic solution, based on the same mesh discretization. The coils were modeled using COMSOL facility to allow a numerical computation of the current density distribution in the coil. Considering 84 turns per coil and the same rms current I_{ph} = 4 A (rated value) for each phase, the current density J [A/mm^2] spatial distribution was determined (Fig. 4), which was then used to compute Joule losses density in [W/m^3]:

$$Q_J = \rho J^2, \quad (7)$$

where ρ [Ωm] is the copper resistivity.

Iron losses. They were computed from the maximum values of the magnetic flux density within the stator iron core. That implied solving a 3D magnetostatic non-linear problem using magnetic potential vector **A** formulation:

$$\mathrm{rot}\left[\nu(\mathbf{B})\cdot\mathrm{rot}\,\mathbf{A}\right] - \mathrm{rot}\,\mathbf{H_c} = \mathbf{J}, \quad (8)$$

where $\nu(\mathbf{B})$ is the magnetic reluctivity which depends on magnetic flux density **B** and $\mathbf{H_c}$ is the coercive magnetic field of permanent magnets.

The spatial distribution of the current density **J** was determined in COMSOL by a numerical computation of the coil geometry (Fig. 4). The phase currents were chosen in such a way to obtain 90° between the axes of the PM field and the armature reaction field, which corresponds to a resistive load.

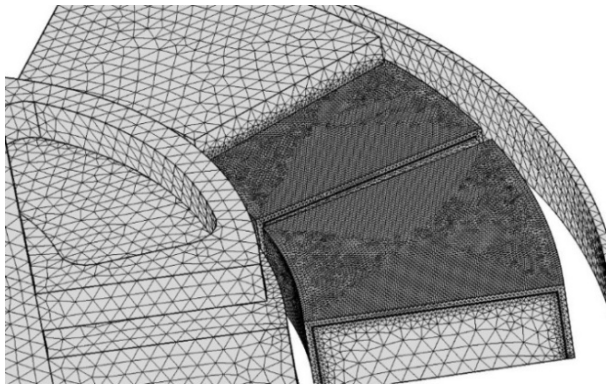

Fig. 3 – Partial representation of the domain discretization – chassis, air and resin regions are removed.

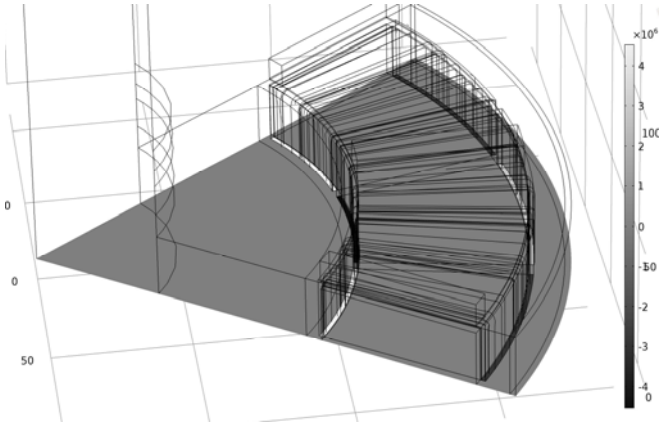

Fig. 4 – Current density lines in the coils – RMS value.

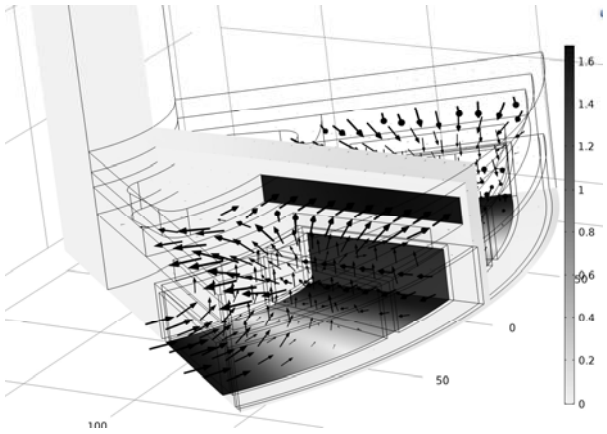

Fig. 5 – Magnetic flux density distribution (gray scale map and vectors) in case of a resistive load and rated current.

The magnetic flux density in the rotor and in the stator iron cores obtained from the numerical solution are in line with the recommended values (Fig. 5). The specific iron losses p_{Fe} [W/kg] were computed by the following model [18]:

$$p_{\mathrm{Fe}} = c_1 B^2 f + c_2 B^2 f^2 + c_3 (Bf)^{3/2}, \quad (12)$$

where the first term corresponds to hysteresis losses, the second to Foucault current losses, and the third to supplementary losses. Coefficients c_1, c_2 and c_3 depend on iron laminations type and they are calculated based on catalogue data. Corresponding to the maximum value of the magnetic flux density B = 1.42 T computed in the iron core and f = 50 Hz, specific losses resulted $p_{Fe} = 2.76 \cdot 10^4$ W/m^3.

Thermal coefficients. In order to create an accurate heat transfer numerical model, the determination of the thermal conductivities and the heat flux coefficients is of paramount importance. That is influenced by thermal conduction anisotropy of certain materials, or by difficulties in identifying correctly the equivalent conductivity of composite materials [19].

The convection coefficient of the outer cooling surface of the studied machine is highly dependent on its geometry and speed of the cooling agent (air). In order to determine the influence of the convection coefficient in this model, several solutions for different coefficients were computed.

In Fig. 6 the dependence of the temperature in the coil against convection coefficient is shown. A conservative value of 10 W/m^2/°C was chosen for the model, this value corresponding to a mild forced convection due to a reasonable wind speed. Noteworthy, the generator output power depends on the wind speed, as well as does the heat generated by the losses in the generator. Equally, higher wind speed will ensure a better cooling of the machine.

In Table 4 are presented the thermal conductivity coefficients for each material used in the studied model.

Another difficult task is to determine the thermal conductivity of the combined copper-air-insulation of the slot composite material. Many researchers proposed simplified models approximating the slot wire distribution with an equivalent conductivity. This is, for usual slot filling factors, about three times larger than air conductivity [11, 20], which is why the coefficient was chosen in this case 0.075 W/m/°C.

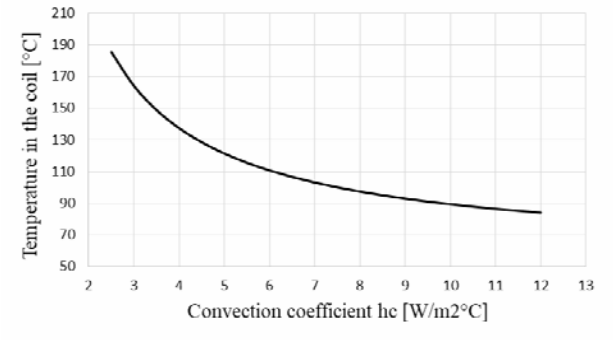

Fig. 6 – Temperature in the iron core *versus* convection heat coefficient.

Table 4

Thermal conductivities of materials used in the model

Material	Thermal conductivity W/m°C	Material	Thermal conductivity W/m°C
air	0.025	magnets	9
slot equivalent	0.075	nylon	0.26
iron chassis	80.2	iron stator stack	21.8
epoxy resin	0.22/1.66		

At the same time, the heat conductivity of the rotor lamination stack is highly anisotropic as it depends on the position of the stack against the heat flux direction. For the iron stack placed with the laminations along Oz axis, parallel to the magnetic field lines like in this model, experimental testing confirms a thermal conductivity of 20 to 40 W/m/°C [21].

The thermal conductivity of the resin used to mechanically enforce the stator coils and for bonding the stator to the chassis, was considered 0.22 W/m/°C (Table 4). That corresponds to a neat epoxy with no special heat transfer properties. However, there are special epoxy materials with enhanced thermal conductivity up to 2 W/m/°C. In order to exemplify the influence of the resin type, subsequent solutions were computed for thermal conductivity values starting from 0.2 to 2 W/m/°C (Fig. 7).

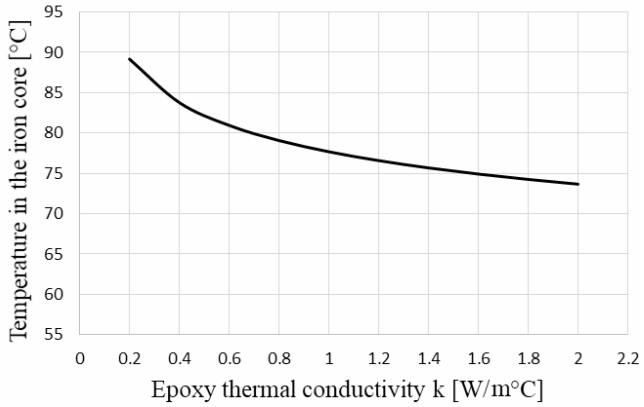

Fig. 7 – Temperature in the stator iron core *vs*. epoxy thermal conductivity.

Steady state models. The results for steady state models are further presented. Variant A and Variant B models yielded rather close results, as seen in Fig. 8 and Fig. 9, respectively. The temperature distribution color maps correspond to nominal Joule and iron losses and an outer heat convection coefficient h_c = 10 W/m^2/°C.

As it can be seen in Variant A, the temperature is not constant in air, while Variant B is based on the assumption that air has uniform temperature inside the generator. Thus, the main differences are in the air regions, the temperatures in the coil, stator iron core or in the chassis having closer values, as in Table 5.

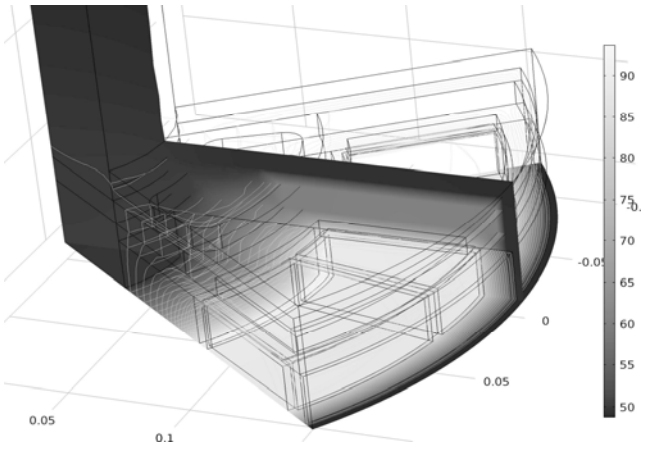

Fig. 8 – Temperature distribution for Variant A model.

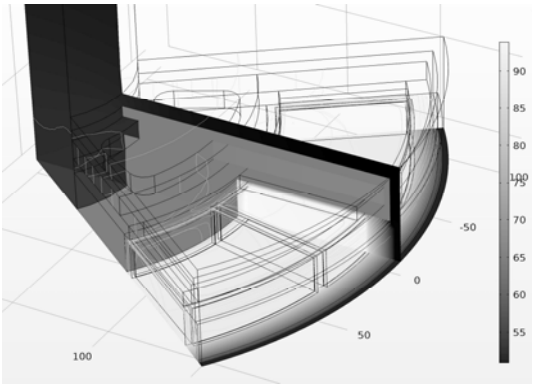

Fig. 9 – Temperature distribution for Variant B model.

Table 5

Temperature values in different points for the two models [°C]

Temperature inside:	*Variant A*	*Variant B*
coil	93.7	93.4
stator iron core	88.65	91.1
rotor yoke	60.3	65.2
chassis	49.2	51.08
shaft	50.7	53.7
air	–	65
magnets	70.9	73.5

Time-dependent models. In addition to steady state models, transient analysis of the heat transfer inside the generator allows estimating the temperature time variation and particularly how fast maximum admissible temperature is reached under given conditions.

This is particularly important in wind generators, as wind speed can increase fast and make the generator exceed its rated power, current and losses. It is thus important to know for how long the machine can operate under a current that exceeds its rated value without being thermally damaged, as well as to find solutions for a better heat extraction that would allow a margin of flexibility in power operation.

The time-dependent temperature variations are shown for different current values (*i.e.* Joule losses) in Fig. 10, using *Variant A* model and considering invariant iron losses. The temperature values shown in Fig. 10a, 10b correspond to the coil and magnets regions, respectively, at their highest temperature points. For a current twice the rated value (*i.e.* $I = 8$A), starting from a temperature of 20 °C, the generator can operate approximately 160 minutes until reaches the maximum temperature of 155 °C.

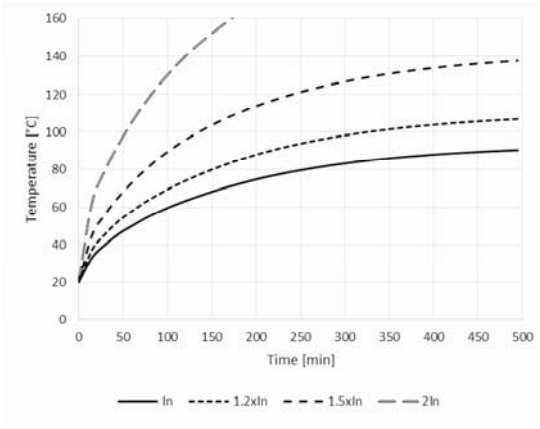

a)

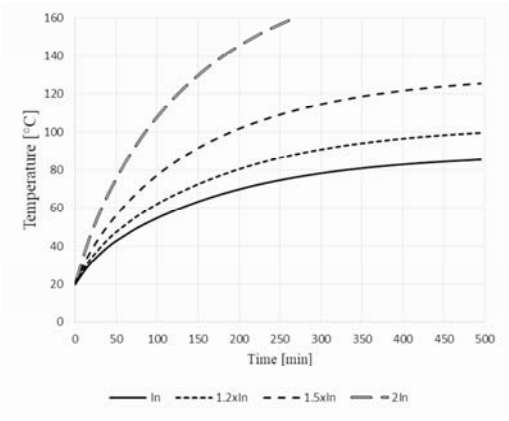

Fig. 10 – Temperature time-variation for different currents: In, $1.2I_n$, $1.5I_n$ and $2I_n$ in the hottest point a) of the coils, b) of the magnets.

The results are also subject to the cooling conditions, particularly the value of the convection coefficient h_c of the outer surface, the resin type, size and its thermal conductivity.

Further on, a model simulating the generator operation at increasingly high wind speeds producing high currents for short periods of times was elaborated. Such a situation may occur in case of small WECS, during strong winds. Above a given wind velocity the turbine is braked by short-circuiting the stator terminals or by overloading the machine.

For the analyzed scenario the current was first considered to be $0.8I_n$ for one hour, assuming the wind having an average speed. Then, the current has a sudden increase to I_n where it remains constant for another half an hour, the average wind speed reaching its rated value. The third stage considers an intermittent variation of the current, with a first linear increase from I_n to $2I_n = 8$ A in one second, then having a linear decrease to I_n in 2 seconds. This intermittent variation corresponds to very strong winds when the wind generator control system intermittently brakes the turbine. This stage lasts half an hour. The temperature variation is plotted in Fig. 11 for temperatures determined in the hottest points of the coils and the magnets. The plots were computed assuming the generator had at start the temperature of 20 °C. The fourth part lasts one hour, during which the current is again $0.8\ I_n$.

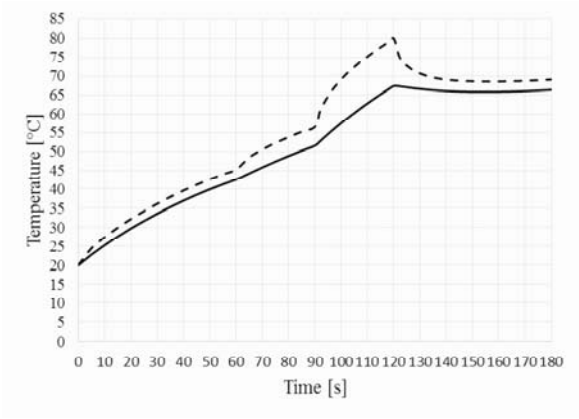

Fig. 11 – Temperature time variation in the hottest point of the coil (dashed line) and in the magnets (continuous line) under different current/Joule losses.

The third stage of the transient heat transfer analysis corresponding an intermittent current was firstly analyzed by considering the real time variation of the current for five

consecutive cycles of three seconds each. A time step of 0.2 s was considered in this case. Then, taking into account the high thermal time constant compared to the electric constant, the model was simulated by considering an equivalent constant electric current producing the same Joule losses during same period of time. In Fig. 12 are plotted the time variations of the temperature for the real time current variation compared to the situation of a constant equivalent current. The temperature increase was practically the same in both situations, confirming that fast current/Joule losses variations can be replaced with equivalent constant currents/ Joule losses, allowing simplification of the model. The plots in Fig. 11 were obtained using the later, simplified model.

Due to variable wind speed, the convection coefficient of the generator outer surface was adjusted to better reflect the cooling conditions: 8 W/m^2/°K when the current is $0.8I_n$, 10 W/m^2/°K for the rated current, and 30 W/m^2/°K during the intermittent current variation period, the stronger the wind the higher the convection.

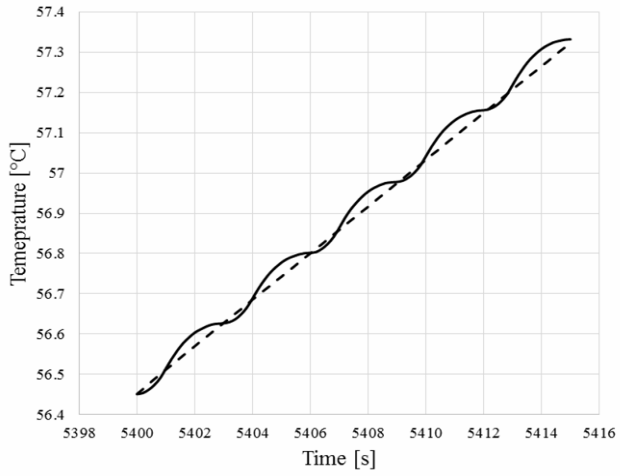

Fig. 12 – Temperature time variation in case of intermittent current computed considering real current variation (solid line) and constant equivalent current (dashed line).

5. CONCLUSIONS

Heat transfer models are very important to determine more precisely the temperature distribution inside electric generators integrated in the WECS. The proposed FEM models allowed obtaining consistent results and a better insight regarding the local temperature distribution than solutions based on equivalent network methods.

An important conclusion of this study is that enclosed generators can be used for WECS as they ensure protection against outdoor factors (rain drops, humidity, corrosion etc.), but heat transfer is less efficient than in less protected machines. At high wind speeds, Joule losses will increase, but the machine cooling gets better due to enhanced convection. Solutions for increased heat extraction could also be an attentive to consider, such as: choosing the proper epoxy resin (having higher thermal conductivity), using coil resin impregnation or larger resin dimensions.

Equally, the heat convection coefficient has a significant importance in the model, while the conductivity coefficient of the composite material of the windings placed inside the slots is less important.

ACKNOWLEDGEMENTS

This paper was elaborated in the framework of the Bridge Grant Programme – PNCDI III, financed by UEFISCDI, project no. 68BG/2016.

The authors thank Multiphysics Modeling Laboratory of UPB for the software support.

Received on May 13, 2017

REFERENCES

1. ***, *Wind in power: 2016 European statistics*, The European Wind Energy Association, 2017.
2. S. Tamalouzt, K. Idjdarene, T. Rekioua, R. Abdessemed, *Direct Torque Control of Wind Turbine Driven Doubly Fed Induction Generator*, Rev. Roum. Sci. Techn. – Électrotechn. et Énerg., **61**, *3*, pp. 244–249 (2016).
3. A. Kerboua, M. Abid, *Hybrid Fuzzy Sliding Mode Control of a Doubly-Fed Induction Generator in Wind Turbines*, Rev. Roum. Sci. Techn. – Électrotechn. et Énerg., **57**, *4*, pp. 412–421 (2012).
4. L. Barote, C. Marinescu, *Modeling and Operational Testing of an Isolated Variable Speed PMSG Wind Turbine with Battery Energy Storage*, Advances in Electrical and Computer Engineering Journal, **12**, *2*, pp. 81–88 (2012).
5. D. Vizireanu, X. Kestelyn, S. Brisset, P. Brochet, Y. Milet, D. Laloy, *Polyphased modular direct-drive wind turbine generator*, European Conference on Power Electronics and Applications, Dresden, Germany, 2005.
6. R. Di Stefano, F. Marignetti, *A Comparison Between Soft Magnetic Cores for Axial Flux PM Synchronous Machines*, Proc. of XXth International Conference on Electrical Machines (ICEM), Marseille, France, 2012, pp. 1922–1927.
7. A. Mahmoudi, H.W. Ping, N.A. Rahim, *A comparison between the TORUS and AFIR axial-flux permanent-magnet machine using finite element analysis*, Proc. of the IEEE International Electric Machines & Drives Conference (IEMDC), Canada, 2011, pp. 242–247.
8. H. Vansompel, *Design of an Energy Efficient Axial Flux Permanent Magnet Machine*, PhD Thesis, Ghent University, Belgium, 2013.
9. *** COMSOL Multiphysics 5.2, Heat Transfer Module User's Guide, 2015.
10. G. Batchelor, *Note on a class of solutions of the Navier–Stokes equations representing steady rotationally-symmetric flow*, Q. J. Mech. Appl. Math., **4**, *1*, pp. 29–41, (1951).
11. D. Staton, A. Boglietti, and A. Cavagnino, *Solving the more difficult aspects of electric motor thermal analysis in small and medium size industrial induction motors*, IEEE Trans. Energy Convers., **20**, *3*, pp. 620–628 (2005).
12. C.H. Lim, J.R. Bumby, R.G. Dominy, G.I. Ingram, K. Mahkamov, N.L. Brown, A. Mebraki and M. Shanel, *2-D Lumped Parameter Thermal Modelling of Axial Flux Permanent Magnet Generators* Proc. of XVIIIth International Conference on Electrical Machines (ICEM), Vilamoura, Portugal, 2008, pp. 1–6.
13. D.A. Howey, A.S. Holmes and K.R. Pullen, *Measurement and CFD prediction of heat transfer in air-cooled disc-type electrical machines*, IEEE Trans. Ind. Appl., **47**, *4*, pp. 1716–1723 (2011).
14. Y.C. Chong, J. Chick, M.A. Mueller, D.A. Staton and A.S. McDonald, *Thermal modelling of a low speed air-cooled axial flux permanent magnet generator*, Proc. of 6th IET International Conference on Power Electronics, Machines & Drives (PEMD), Bristol, UK, 2012, pp. 1–7.
15. A.F. Mills, *Heat Transfer,* Prentice Hall, 1999.
16. D.A. Howey, P.R.N. Childs, A.S. Holmes, *Air-Gap Convection in Rotating Electrical Machines*, IEEE Trans on Industrial Electronics, **59**, *3*, pp. 1367–1375 (2012).
17. J. Owen and R. Rogers, *Flow and Heat Transfer in Rotating-Disc Systems*, Vol. 1: *Rotor–Stator Systems*, 1st ed. Taunton, U.K.: Res. Stud. Press, 1989.
18. ***Cedrat: *User guide Flux® 11*, 2015.
19. D. Staton, L. Šušnjić, *Induction Motors Thermal Analysis*, Strojarstvo, **51**, *6*, pp. 623–631 (2009).
20. A. Boglietti, A. Cavagnino, M. Lazzari, M. Pastorelli, *A Simplified Thermal Model for Variable Speed Self Cooled Industrial Induction Motor*, Proc. of IEEE IAS Annual Meeting, 2002, USA.
21. S.K. Pal, *Heat Transfer in Electrical Machines – A Critical Review*, ERA Report No 71–76, July, 1971.